Inter-ion Coulomb interactions in a Magneto-Optical Trap Ion Source

A.V. Steele, B. Knuffman, and J. J. McClelland

Center for Nanoscale Sciences and Technology, National Institute of Standards and Technology

Gaithersburg, MD 20899 USA

ABSTRACT

We have investigated the role played by inter-ion Coulomb interactions in a magneto-optical trap ion source (MOTIS). Using a Monte Carlo simulation accounting for all pair-wise ion-ion Coulomb interactions in the source, we have calculated the broadening of the transverse spatial and velocity distributions as well as the increase in emittance over a range of beam currents and extraction electric fields. Using a ^{7}Li MOTIS, we have experimentally studied the broadening of the spatial distribution as a function of total beam current and extraction electric field by measuring the fraction of the beam current that passes through a 20 μm diameter aperture. The Monte Carlo simulations agree well with the experimental results, indicating that such simulations capture the essential physics of the source. Our results show that while Coulomb interactions can cause a significant increase in emittance in some situations, it is possible to keep the effects to an acceptable level by suitable choice of extraction field and beam current. These considerations are essential to the process of optimizing MOTIS geometry and operating conditions for use in high-resolution focused ion beam applications.

I. Introduction

Over the past three decades, the use of focused ion beams (FIBs) has become widespread in applications such as nanoscale milling, deposition, and imaging. Based predominantly on the very robust and simple gallium-based liquid metal ion source (LMIS), a number of commercial instruments are currently available that can create structures with nanoscale precision, removing or adding material through ion

bombardment or beam-induced chemistry. Imaging with the ion beams in these systems is also

possible, although high-resolution images are difficult to obtain because of sample damage that occurs

when the beam is focused to the nanometer scale, resulting in a current density in the focused spot that

can reach as high as 10 A cm^{-2}.

In the past few years, interest in focused ion beams has seen a marked increase due to the development

of several new ion sources that promise to dramatically expand the capabilities of these instruments.

Key to the usefulness of these new sources is an ability to produce a number of different ionic species

while maintaining a brightness and an emittance that are commensurate with nanoscale focusing.

Expanding the choice of ionic species beyond gallium makes possible a wide variety of new applications,

ranging from contamination-free milling to damage-free and enhanced-contrast imaging. The gas field

ionization source (GFIS), in which a gas is ionized in the high field of a very sharp tip, is one example of a

new source that has seen significant success [1].   With this source, the replacement of heavy Ga$^+$ ions

with light He$^+$ ions has enabled very high resolution imaging with minimal sample damage. An

inductively-coupled plasma source [2] has also shown great promise for contamination-free milling,

producing Ar$^+$ or Xe$^+$ ion beams that can remove material efficiently.

The magneto-optical trap ion source (MOTIS) promises to expand the choice of ions available for FIB

applications well beyond those available with GFIS or plasma sources. Based on ionization of laser-

cooled neutral atoms, the MOTIS can in principle be configured to produce ions of over 20 different

elements[3]. Obtaining its high brightness from the very cold temperature (a few hundred microkelvin)

that the ions have when they are produced, rather than from confining the emission to a very small

region, the MOTIS has a number of advantages. For example, forming a probe involves imaging a virtual

source with demagnification of up to 2500X, making the probe far less sensitive to the vibrations and

instabilities one typically sees with a point-like ion source.   Further advantages include a large degree of control over the energy spread of the beam, isotope selectivity, and an ability to produce single ions "on demand" [4].

While a focused probe system has only very recently been demonstrated using a MOTIS [3], a number of studies of the source have been carried out. Several theoretical analyses of the performance of this type of source have been presented [5,6,7], including a detailed treatment of Coulomb interactions [8], and these indicate that the emittance and brightness are in a range that is attractive for a number of applications. Measurements of the emittance of a Cr MOTIS [9] have shown that it can be as small as 6×10^{-7} mm mrad (MeV)$^{1/2}$, a value that is as good as, or even slightly better than, the LMIS. Measurements on a Rb MOTIS showed that when used in a pulsed mode, very low energy spread bunches of ions could be produced [10].

In this paper we discuss calculations and measurements carried out on a Li MOTIS in anticipation of adapting this source to a focused ion beam system. Our main goal is to investigate the effects of Coulomb interactions on the transverse velocity spread, the spatial distribution of the ion beam, and ultimately the emittance in order to determine the ion currents and extraction fields where these effects are significant, and what steps can be taken to minimize them. The low emittance of a MOTIS depends primarily on source ions having a small velocity spread transverse to the beam's propagation; in the absence of Coulomb interactions this spread is determined by the temperature of the neutral atoms in the MOT. Therefore, source emittance will be degraded if Coulombic forces heat the ions to a temperature larger than that of these atoms. Although the MOTIS has a charge density in the ion creation region that is much smaller than any point-like source, Coulomb interactions can still be significant if the charge density is high enough.

The geometry of the Li MOTIS under consideration here is shown in Fig. 1a. Based on earlier Cr MOTIS realizations [3,7], the source consists of a magneto-optical trap (MOT) located between two electrodes separated by 10 mm. One electrode is a mirrored plate with an extraction hole, and the other is a transparent indium tin oxide-coated window. The MOT is formed by four laser beams incident at 45° to the electrode surfaces, and one more retroreflected laser beam perpendicular to these beams, together with a quadrupole magnetic field created by two permanent magnets. Loading of the MOT is achieved via a beam of slow neutral Li atoms produced by an atomic beam source oven and a Zeeman slower [11] (not shown in the figure). An ionization laser incident through the transparent electrode along the ion beam axis creates ions, and these are extracted from the ionization region of the MOT by applying a voltage across the two electrodes, which accelerates them into a beam that exits the source through the hole in the bottom electrode.

We note that the "axial ionization" mode described above, and schematically illustrated in Fig. 1b, is not the only viable MOTIS single-beam ionization configuration. One alternative is to pass the ionization beam through the MOT transverse to the beam's propagation axis. The current density in an ion beam formed in this way is much lower, and the effects of Coulomb interactions are significantly reduced. However, we have chosen to study the axial mode for the present work for several reasons. First, axial ionization allows for a simpler system since it results in an axially symmetric ion beam without the necessity of a beam limiting aperture. Second, a larger beam current density is possible because all the ions created over the entire length of the ionization region contribute to the ion beam and are confined to a small cross sectional area. Third, since the purpose of this study is to examine Coulomb interactions, we chose the ionization mode that would yield the most dramatic effects. In using a MOTIS

4

for a given application, of course, either mode can be used, depending on the desired beam characteristics.

II. Coulomb interaction calculations

In order to explore the effects that Coulomb interactions can have on the ion beam characteristics as a function of extraction field and beam current, we performed a series of Monte-Carlo (MC) simulations of the MOTIS, tracking all inter-ion Coulomb forces and generating predictions of transverse velocity distributions, emittance, and spatial spreading. There exists an enormous body of work analyzing the effects of inter-ion forces in charged particle beams [12]. For point-like sources with a high charge density at the point of ion creation, such as the LMIS, an approach that considers every set of pair-wise particle Coulomb forces is not tractable. For such sources a variety of space-charge and so-called "statistical Coulomb" approximations may be employed to estimate phase-space evolution.   While these analytical approaches can be highly effective in predicting beam behaviors, some effects only appear when the full N-body problem is solved for all of the ions in the beam.   In the MOTIS the particle number and density remain low enough that a numerical solution of the full problem becomes tractable. For example, in a 12 pA beam where ionized lithium atoms are accelerated from rest to 25 eV over a distance of 6 mm, only about 35 ions will be present in the beam at a time.

In our simulation, ions are continuously created in a Poisson process with an expectation time between particle creations commensurate with the desired beam current. The created ions are given a three-dimensional Gaussian initial velocity distribution with equal standard deviations in all three directions of $\Delta v_{x,y,z} = \sqrt{k_B T / m}$, where z refers to the ion beam axis, x and y are transverse directions, T is the ion temperature, m is the ion mass, and k_B is Boltzmann's constant. The initial positions of the ions are

chosen from Gaussian distributions as well, with standard deviations $\Delta z = \sigma_{MOT}$, the standard

deviation of the cold atom cloud, and $\Delta x, \Delta y = \sigma_{beam}$, the standard deviation of the ionization laser

beam. In the weak ionization regime, where the local ion production rate is not limited by diffusion of

particles into the ionization beam [8], these Gaussian distributions should be an accurate representation

of the initial conditions in the MOTIS. Once the ions are created, their equations of motion are

integrated as they are accelerated by a constant, uniform electric field along the z-direction and by their

pair-wise interactions with all of the other ions in the system. After traveling a desired distance, ions are

removed from the system and their positions and velocities are recorded. The electric field in the

calculation is strictly uniform along the z axis, with no consideration of any fringe fields or lensing from

apertures. This simplification ensures that all effects seen in the calculations can be attributed solely to

ion-ion interactions. The integration time step required for an accurate simulation depends on the

particle density, beam currents and accelerating electric field applied. For all the simulations presented

here, we verified the convergence of our results as a function of time step. Typical simulations require

about 8 minutes to run 20 000 ions through the system using a single processor.

The emphasis of our simulations was the impact of Coulomb interactions in a MOTIS source when

compared with an identical source with no Coulomb effects. The strength of the inter-ion forces will be

greatest in regions of high charge density, and in a MOTIS this region will be near to the overlap

between the MOT and the ionization laser. Therefore, we chose to focus on the effects of two

parameters which have a large impact on the charge density near the source, namely the extraction

electric field and beam current. Higher current means more ions in the system and increased Coulomb

interactions. Larger extraction fields result in more rapid acceleration of the ions, and an associated

more rapid decrease in charge density as the ions leave the creation region, thus reducing Coulomb

effects.

Fig. 2a shows a series of transverse velocity histograms for a 12 pA Li ion beam that has been accelerated over a distance of 6 mm in a number of different uniform extraction electric fields. The top curve shows the initial velocity distribution inherited from the 1 mK thermal atomic cloud, and the lower curves show how this initial distribution is broadened by Coulomb interactions during the acceleration. While substantial broadening of the transverse velocity distribution is apparent at the lower extraction fields, the higher extraction fields appear to reduce this effect. Fig. 2b shows the dependence of the velocity spreading on beam current. The curves represent currents of between 4.5 pA and 30 pA in ion beams accelerated by a fixed extraction electric field of 12 kV/m. As in Fig. 2a, a broadening of the transverse velocity distribution is seen. In this case the broadening is relatively minor at the lower currents and becomes quite large at the higher currents.

To gain further insight into the role played by Coulomb interactions, we sought to answer the question of whether the velocity broadening seen in Fig. 2 occurs over the length of the beam acceleration region or only within small a volume near the ion creation region. Fig. 3a shows the evolution of the transverse velocity distribution of a 12 pA beam accelerated in a 12 kV/m field at selected points along the z axis. As seen in the figure, almost all the heating happens within the first 1.5 mm of propagation, with only a small change occurring in the final 4.5 mm. Fig. 3b illustrates this phenomenon further by showing the evolution of the beam's emittance as it propagates along the 6 mm, where we have used the standard definition for normalized rms-emittance [13], given by

$$\varepsilon_{\text{rms}} = \sqrt{\left\langle x^2 \right\rangle \left\langle x'^2 \right\rangle - \left\langle xx' \right\rangle^2} \sqrt{U},\tag{1}$$

where x is the transverse position, x' is the transverse angle, and U is the kinetic energy. Here we see the emittance rising rapidly in the first millimeter or so, and then rising more slowly as the beam

continues to be accelerated.   This early rapid increase in emittance can be understood by noting that

the charge density is highest when the ion velocities are low.

In generating the curve in Fig. 3b we found that, because the emittance definition (1) is strongly

influenced by particles on the periphery of phase space, a few outliers in the simulation added a large

amount of noise to the emittance values.   To remove this artifact, we culled ions with the highest

velocities (amounting to 1% or fewer of the total ions) from the distributions before calculating the

emittance. While this culling may hamper our ability to predict a very weak halo around the beam, we

note that such a halo containing less than 1% of the total current would only have a limited impact on

performance in most FIB applications.

In the MOTIS, the initial normalized rms emittance can be obtained from fundamental source properties

via [7]

$$\varepsilon_x = \Delta x \sqrt{k_B T / 2} \,. \tag{2}$$

For the simulations shown in Figs. 2 and 3, where $\Delta x = 4.1 \ \mu\mathrm{m}$ and $T = 1 \ \mathrm{mK}$, we find

$\varepsilon_x = 8.5 \times 10^{-7} \ \mathrm{mm \ mrad} \ \sqrt{\mathrm{MeV}}$. In Fig. 3b, we see that the emittance from our calculation starts

very close to this value, before increasing as a result of Coulomb interactions. The slight discrepancy at

$z = 0$ arises because the spatial distribution is Gaussian along z, and half of the atoms created will be

initially at positions $z < 0$. The Coulomb forces experienced by these ions as they travel from their

initial positions to the $z = 0$ point result in the beam having an increased emittance even at the origin.

The cause of the velocity histograms widening in Figs 2 and 3a can be roughly categorized as either

being due to space charge or to so-called statistical Coulomb effects [12]. Space charge forces will

dictate the evolution of a beam where the charge of the constituent particles has been smoothed over

8

the entire beam. Statistical Coulomb effects are random in nature and arise from the inherent

discreteness of charge in the ion beam. The space charge forces will give rise to beam defocusing,

creating (not necessarily linear) correlations between ion positions and velocities. Therefore, while a

beam affected by space charge would see a large broadening of its velocity spread, its emittance would

not increase in proportion to that broadening. Conversely, velocity spreading which was due to random,

statistical Coulomb forces would cause an irreversible increase in beam emittance. Figure 4 illustrates

the difference between these two types of velocity spreading. The black dots in the phase space plot

are 1000 ions taken from a simulated beam of 30 pA at an extraction electric field of 12 kV/m. Initial

positions and velocities are in green; final coordinates are in black. The tilt in the final distribution is the

result of correlations between transverse position coordinate x and velocity v_x. We note that our model

does not include any field curvature, so these correlations are purely due to inter-ion forces. Linear

correlations can be removed by applying a simple transformation similar to the action of an ideal lens;

each ion has its velocity changed in proportion to its position coordinate, with the constant of

proportionality chosen such that $\langle xv_x \rangle = 0$. The residual velocity spread, shown in magenta, gives a

more accurate picture of the nonlinear forces and irreversible heating the ion beam has experienced.

From the histograms in Fig 4b., it is clear that in addition to linear space charge forces, nonlinear forces

and/or statistical Coulomb effects are present in the beam.

Having seen the effects of Coulomb interactions on the emittance of the source in Fig 3b., we can now

examine the practical question of what range of operating conditions are best for minimizing these

effects. To address this question, we have calculated the emittance for a large number of simulations

with beam currents ranging from 0.2 pA to 100 pA and extraction fields ranging from 0.6 kV/m and 160

kV/m. The results of these calculations are shown in Fig. 5. This plot allows predictions to be made

about how this source will perform in different regimes. For example, if an emittance of less than 5 x

10^{-6} mm mrad (MeV)$^{1/2}$ at a current of 10 pA is desired, the plot shows that an extraction field of 10 kV/m or higher is required.

From Fig. 5 it is evident that for any current it is possible to choose an extraction field that will make the Coulomb effects negligible. However, it is important to note that a higher extraction field may lead to an unfavorable longitudinal energy spread in the ion beam. Since the ions are created in an extended region with standard deviation Δz, their energies will have a distribution with a standard deviation $\Delta U = \Delta z E$, where E is the extraction field. This spread can be significant in some situations. For example, with the source geometry discussed in this paper, a 10 kV/m extraction field would result in $\Delta U = 2.5$ eV, a value that is much larger than the inherent 80 neV arising from the ion temperature (but approximately the same as a LMIS). This additional energy spread will most likely necessitate a trade-off between increased source emittance and chromatic aberrations when running the MOTIS at high currents. It is also worth recalling that the results in Fig. 5 only hold for a Li ion source using axial ionization in the particular source geometry discussed in this paper. Sources with different geometries, dimensions, ionization schemes and ionic species may have more or less severe effects.

III. Experiment

In order to validate the Monte Carlo simulations discussed in section II, we conducted a series of measurements in a Li MOTIS with operating conditions corresponding to those chosen for the calculations. For an ideal comparison, one might consider making a range of emittance measurements corresponding to the points shown in Fig. 5, covering a good portion of the current and extraction field parameter space displayed in the figure. However, the emittances expected in such a measurement series are quite small, and are therefore difficult to measure. In particular, correlations between angle

and position, which must be removed to obtain a true emittance, cannot easily be obtained.

Furthermore, if the goal is validation of the Coulomb-interaction predictions of the calculations, it is

sufficient to measure a quantity that is sensitive to these interactions over a range of source parameter

values. Based on these considerations, we have chosen to measure the amount of current that passes

through a 20 μm diameter aperture placed just beyond the extraction hole in the mirrored electrode of

the MOTIS. In the absence of Coulomb interactions, one would expect the fraction of current passing

through this aperture to be independent of total beam current. In addition, it should be independent of

extraction field as long as the initial thermal velocities are small and any lensing action in the extraction

process is negligible. In the presence of Coulomb interactions, however, as predicted by our

simulations, higher currents and lower extraction fields will lead to spreading of the beam, and a smaller

fraction passing through the aperture. Observing this transmitted current fraction thus provides us with

a simple measurement that can be compared directly with the simulations.

The geometry of the MOTIS experiment is shown in Fig. 1. Laser light for cooling and trapping the Li

atoms was produced by a diode-laser-seeded tapered-amplifier (master oscillator power amplifier

combination). The laser system included a repumping component generated by splitting off

approximately 50 % of the laser power, shifting the frequency by 800 MHz with an acousto-optical

modulator, and recombining via an optical fiber coupler array, which was also used to distribute the

laser light into the various beams for the experiment. The MOT beams were tuned just below the 2s

$^2S_{1/2}$ – 3p $^2P_{3/2}$ resonant absorption line in Li at 671 nm, and typically had $1/e^2$ diameters of 4 mm and

powers of 1.5 mW. The laser beam used in the Zeeman slower was shifted by 500 MHz to 600 MHz with

an acousto-optical modulator and further amplified by a second tapered amplifier system, resulting in a

typical power of 100 mW in a 10 mm $1/e^2$ diameter beam. The quadrupole magnetic field, formed by

two opposing stacks of NdFeB permanent magnets located in the vacuum system just outside the

electrodes, had a gradient of 0.46 T/m perpendicular to the ion beam axis and 0.23 T/m along the ion beam axis. Under these conditions the MOT had a typical size (one standard deviation) of 250 μm, a typical load rate of 2 x 10^8 s^{-1}, a typical steady state population (without ionization) of 2 x 10^7 atoms, and a typical temperature of 1 mK. The ionization laser, produced by a frequency-doubled single-frequency continuous-wave Ti-sapphire laser, had a wavelength of 350 nm and was focused on the MOT center along the direction of ion beam propagation, with typical beam waist 1/e^2 diameter of 16.4 μm and power up to 10 mW. Varying the power in this laser beam allowed us to produce any desired current in the ion beam, from below 1 pA to over 30 pA.

The extraction electric field E was produced by applying the appropriate voltage to the transparent electrode, which was separated by 10 mm from the grounded mirror electrode. The central 50 mm of the mirror electrode consisted of a 100 μm thick Si wafer coated with aluminum, at the center of which was the 4 mm extraction hole. The 20 μm aperture, also kept at ground potential, was located directly below this wafer at a distance of 1 mm from the wafer surface, making its location 6 mm from the center of the ionization volume in the MOT (see Fig. 1).

Of the total ion current I_{total} present in the beam, the amount of current I_{ap} that passed through the aperture was collected by a plate held at ground potential, located 9 mm beyond the aperture. I_{total} was measured by collecting current on a cone-shaped electrode that could be inserted between the mirrored and transparent electrodes (see Fig. 1a). In order to direct the beam toward the cone during this experiment, the mirrored and transparent electrodes were held at +50 V relative to the grounded cone. All current measurements for both I_{total} and I_{ap} were obtained with a picoammeter, and had an estimated one-standard-deviation uncertainty of $\pm$ 5 %[14] of the measured value, due largely to small

random fluctuations of the current reading. As a result, the calculated beam current fractions I_{ap}/I_{total} had an uncertainty of $\pm$ 7 %. To verify that the current collection efficiency was the same on the current-collecting plate and in the cone, we replaced the 20 µm aperture with a 100 µm aperture so that all current in the beam could easily pass through to the collection plate; currents measured in both places were the same within the measurement uncertainty. This being the case, systematic errors due to the absolute ion beam current collection efficiency and calibration of the picoammeter effectively canceled in the determination of the beam fraction.

In Fig. 6, we show the measured fraction of the beam current I_{ap}/I_{total} that passed through the 20 µm aperture as a function of the extraction electric field E for various values of the total current I_{total}. For each value of the total current, the beam fraction exhibits a similar trend as a function of the extraction electric field. At low extraction fields the transmitted beam fraction is quite low. As the extraction field increases, the measured beam fraction increases monotonically, approaching an asymptotic maximum value. For higher beam currents, the transmitted fraction is smaller for a given extraction field, and the field required to reach the asymptotic value is larger.

Also shown in Fig. 6 are results from MC simulations carried out with beam current and extraction field values corresponding to the experiment. These results were obtained by calculating the ion spatial distribution after a propagation distance of 6 mm, and determining what fraction of the ions had lateral positions within a diameter of 20 µm. As seen in the figure, we find excellent agreement between simulations and the experimental results for all currents and extraction fields.

We note that in order to compare the simulation results with the experiments, we found it necessary to uniformly scale all the simulated beam fractions by a factor of 0.75. This scaling was considered

appropriate because, while the simulations predicted an asymptotic transmitted beam fraction of

approximately 0.94, every beam current fraction measured attained an asymptotic value of only 0.7

(within the uncertainty of the measurement) when a large enough extraction field was applied. We do

not believe that the discrepancy arises due to a velocity-spread related expansion of the spatial

distribution of the ion beam, such as those produced by inter-ion Coulomb interactions, because the

measured value of the beam fraction remains constant over the extraction field range tested of 12 kV/m

to 100 kV/m (not shown in Fig. 6).

While we do not have a definitive explanation for the 25 % difference in absolute scale factor between

the simulations and the experiment, the following effects, which are not included in the MC model of

the experiment, could contribute to this difference. (1) Since the ionization volume in the MOTIS has a

large aspect ratio of $\sigma_{\mathrm{MOT}}/\sigma_{\mathrm{beam}} = 60$, deviation from perfect alignment of the long axis of this

ionization volume with the extraction field direction could reduce the transmission of the aperture.

Calculations show this reduction to be approximately 10 % per degree of misalignment, for small angles.

(2) Local modification of the atomic density profile in the MOT due to the ionization process could result

in an initial ion distribution that does not match the laser beam intensity profile. This effect is difficult to

estimate, although we believe it is small because we are in the weak ionization regime. (3) Even though

the 20 μm aperture is located only 1 mm downstream of the 4 mm hole in the mirror electrode, and the

aperture and the mirror electrode are held at the same potential, there is nevertheless a very weak lens

formed in this region which distorts the beam slightly on its way to the aperture. According to ion

trajectory simulations, this lensing could account for a 2 % reduction in the transmitted current.

Additionally, the lensing at the small aperture is negligible. (4) Whereas the simulation assumes a

Gaussian ionization laser beam with uniform width for the entire length of the ionization region, in fact

the Gaussian beam width increases slightly at each end of the region because the beam is passing

through a focus. Estimates show this could account for an approximately 3 % reduction in transmission through the aperture in the experiment.

Using insights gained from the Monte Carlo simulations, we can interpret the beam fraction trend with electric field seen in Fig. 6 in terms of the ion-ion Coulomb interactions. For low extraction fields, the ion-ion interactions in the source lead to a large spread in the transverse velocity distribution of the ions (see Fig 3a), and the time of flight from the source to the aperture is relatively long. Thus, the ion distribution expands appreciably, reducing the fraction of ions that pass the beam defining aperture. As the electric field is increased, both the transverse velocity spread in the ion beam and the time of flight are reduced, resulting in less beam spreading and an increase in the fraction of atoms passing the aperture. At large enough electric fields, the time of flight is not long enough for the beam to expand appreciably and the beam fraction approaches an asymptotic maximum.

The trend with beam current can also be understood in terms of the ion-ion Coulomb interactions. As the total beam current is increased, the respective I_{ap} / I_{total} vs. E curves in Fig. 6 shift to larger extraction electric fields. For a given extraction electric field, the fraction of current passing the aperture is inversely related to the total beam current. This behavior stems solely from the fact that the strength of the ion-ion interactions is larger in higher density beams, resulting in relatively larger amounts of heating (clearly visible in Fig. 3b) and beam expansion during propagation.

IV. Conclusions

We have analyzed the effects of ion-ion Coulomb interactions on the position and velocity distributions of a MOTIS ion beam. Using a MC simulation, which tracks the evolution of ions as they are created and accelerated in a constant electric field, we have predicted the beam velocity spread, emittance, and

spatial spread over a range of different beam currents and electric fields for a specific MOTIS geometry in axial ionization mode. The results of the simulations indicate that at higher beam currents and weaker electric fields, the transverse velocity spread and emittance will rise substantially above the interaction-free values. The simulations also indicate that the Coulomb effects are concentrated in the first few of millimeters of the ion's flight. We have verified the accuracy of the simulations by comparing the predictions to measurements of the beam current passing through a 20 μm diameter aperture placed 6 mm from the center of a ^{7}Li MOTIS. We found that our uniformly scaled simulation results successfully predicted the experimental measurements collected over a range of beam currents and extraction electric fields.

We conclude that Coulomb interactions can have a significant effect on MOTIS emittance when the source is operated in axial mode. However, this effect can be mitigated by ensuring that the extraction electric field at the source is sufficiently high, and by using a beam current that is not too high. For a Li source with our specific geometry, the electric fields and currents required to keep the effects of Coulomb interactions to an acceptable level result in a source with excellent operating characteristics: an emittance in the range of 10^{-6} mm mrad (MeV)$^{1/2}$, currents of several pA, and an energy spread of a few eV. MOTIS performance will be affected by a number of parameters: the fundamental source emittance (governed by source size and ion temperature), possible emittance increases due to Coulomb interactions, longitudinal energy spread arising from the extraction electric field, and source geometry. Accounting for tradeoffs among all of these parameters will be required to achieve the smallest focused probe size in a fully optimized MOTIS-based FIB system.

Acknowledgements

Manuscript accepted for publication in Appl. Phys. Lett.

References

[1]B. W. Ward, J. A. Notte, and N. P. Economou, J. Vac. Sci. Technol. B **24**, 2871-2874 (2006).

[2]N. S. Smith, W. P. Skoczylas, S. M. Kellogg, D. E. Kinion, P. P. Tesch, O. Sutherland, A. Aanesland, and R. W. Boswell, J. Vac Sci. Technol. B **24**, 2902-2906 (2006).

[3]A. V. Steele, B. Knuffman, J. J. McClelland and J. Orloff, J. Vac. Sci. Technol. B **28**, C6F1 (2010).

[4]S. B. Hill and J. J. McClelland, Appl. Phys. Lett. **82**, 3028 (2003).

[5]B. G. Freinkman, A. V. Eletskii, and S. I. Zaitsev, Microelectron. Eng. **73**, 139-143 (2004).

[6]B. J. Claessens, S. B. van der Geer, G. Taban, and E. J. D. Vredenbregt, Phys. Rev. Lett. **95**, 164801 (2005).

[7]J. L. Hanssen, J. J. McClelland, E. A. Dakin, and M. Jacka, Phys. Rev. A **74**, 063416 (2006).

[8]S. B. van der Geer, M. P. Reijnders, M. J. de Loos, E. J. D. Vredenbregt, P. H. A. Mutsaers, and O. J. Luiten, J. Appl. Phys. **102**, 094312 (2007).

[9]J. L. Hanssen, S. B. Hill., J. Orloff and J. J. McClelland Nano Letters **8**, 2844-2850 (2008).

[10]M. P. Reijnders, P. A. van Kruisbergen, G. Taban, S. B. van der Geer, P. H. A. Mutsaers, E. J. D. Vredenbregt, and O. J. Luiten, Phys. Rev. Lett. **102**, 034802 (2009).

[11]U. Schünermann, H. Engler, M. Zielonkowski, M. Weidemüller, and R. Grimm, Opt. Commun. **158**, 263-272 (1998).

[12]for a review see: P. Kruit and G.H. Jansen, in *Handbook of Charged Particle Optics*, edited by J Orloff(CRC Press, Florida, 2009). and included references

[13]M. Reiser, *Theory and Design of Charged Particle Beams*, (Wiley-VCH, Weinheim, 2008).

[14] Unless otherwise specified, all uncertainties in this paper are intended to be interpreted as one-standard-deviation, combined standard uncertainty.

FIGURE CAPTIONS

FIG 1. (a) Cross-sectional view of the MOTIS geometry. Two pairs of counter-propagating laser beams (MOT lasers) pass through a transparent electrode and are reflected by a mirror electrode. The spacing between these electrodes is 10 mm. At the intersection of these four beams another counter-propagating beam pair runs perpendicular to the figure. This intersection is half way between the two electrodes. Two opposing permanent magnets also lie along the axis perpendicular to the page, creating a quadrupole field. An ionization laser beam is incident along the ion beam axis. Photoionized atoms are extracted from the MOT by a voltage applied to the transparent electrode, and are accelerated through a 4 mm diameter hole in the mirror electrode. A 20 μm aperture is placed 1 mm below the mirror electrode, and current passing through this aperture is collected on a plate. Alternatively, the total beam current can be collected on a movable cone-shaped electrode inserted between the transparent and mirrored electrode. To direct the beam to the cone-shaped electrode, the mirror and transparent electrodes are held at +50 V relative to the grounded cone. (b) Detailed view of ionization region. Cold trapped lithium atoms in the MOT (red) are ionized by a UV laser (violet) and accelerated by the electric field in the source region to form the ion beam (yellow) with total current I_{total}. The amount of current that passes through the 20 μm aperture is I_{ap}.

FIG 2. Transverse velocity histograms generated by Monte Carlo simulations. (a) Broadening of the transverse velocity distribution after 6 mm of flight as a function of electric field at the ion source. The lithium ions have an initial velocity distribution derived from a temperature of 1 mK. In each curve a 12 pA ion beam is being accelerated by a uniform electric field. The initial spatial distribution is

Gaussian with standard deviations $\Delta x, \Delta y = 4.1\,\mu$m and $\Delta z = 250\,\mu$m. (b) As in (a) but now holding the

extraction electric field fixed at 12 kV/m and varying the beam current. 20000 ions were run through

the system for each curve.

FIG 3. Monte Carlo simulated changes in transverse velocity and beam emittance as a function of

distance from the center of the MOTIS along the beam propagation axis. (a) Perturbation of an initial

velocity distribution as a function of distance from center of the source. Top curve represents a 1 mK

lithium atom velocity distribution. Lower curves are simulations of a 12 pA beam being accelerated by a

12 kV/m electric field over the distances of 1.5 mm and 6 mm. The initial spatial distribution is as in Fig.

2. 400 000 ions were run through the system for each curve. (b) Evolution of beam emittance as a

function of distance from the MOT center. Inter-ion Coulomb interactions cause the beam's emittance

to increase over its propagation.

FIG 4. Phase space plots and velocity histograms for beam with 30 pA and an extraction electric field of

12 kV/m (corresponding to the 30 pA simulation in Fig. 2(b)). The initial conditions are in green. The

results after the ions have traveled 6 mm are in black. The black dots after the application of a

transformation to remove linear correlations between the position and velocity coordinate are in

magenta. (a) Transverse coordinate velocity and position phase space graph for 1000 selected ions from

a simulation of 20000 ions. (b) Velocity histograms for the same ions shown in (a). Their maxima have

been normalized to more easily show the differences in curve width.

FIG 5. Monte Carlo simulated beam emittance for selected currents as a function of extraction electric

field E. MOTIS geometry and temperature of the source are the same as in Figs. 1-3. At higher

currents and at lower extraction electric fields the final emittance after being accelerated over 6 mm is

larger than the interaction-free value. However, for a sufficiently high extraction field, all beam currents converge to the interaction-free emittance value.

FIG 6. Fraction of beam current passing a 20 μm aperture vs extraction electric field for various beam currents. Symbols are experimental data and solid lines are Monte Carlo simulations. Uncertainties of the measured data are ± 7 %.
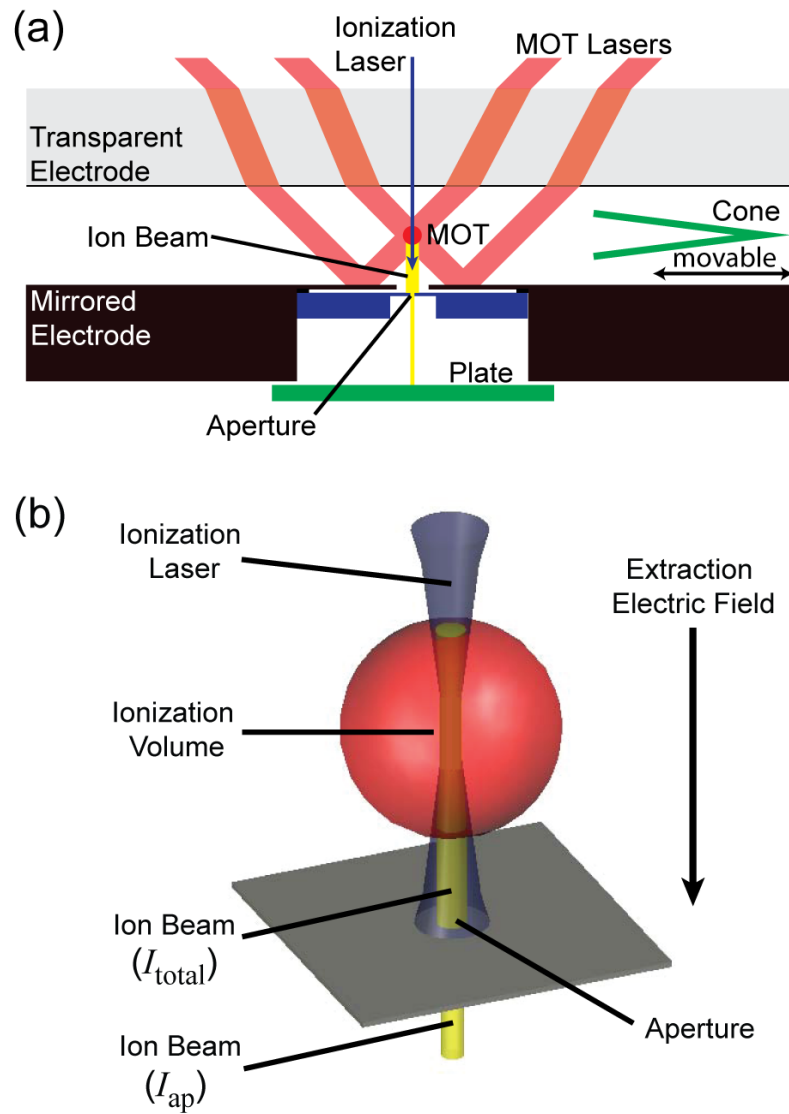
FIG 1. (a) Cross-sectional view of the MOTIS geometry. Two pairs of counter-propagating laser beams (MOT lasers) pass through a transparent electrode and are reflected by a mirror electrode. The spacing between these electrodes is 10 mm. At the intersection of these four beams another counter-propagating beam pair runs perpendicular to the figure. This intersection is half way between the two electrodes. Two opposing permanent magnets also lie along the axis perpendicular to the page, creating a quadrupole field. An ionization laser beam is incident along the ion beam axis. Photoionized atoms are extracted from the MOT by a voltage applied to the transparent electrode, and are accelerated through a 4 mm diameter hole in the mirror electrode. A 20 µm aperture is placed 1 mm below the mirror electrode, and current passing through this aperture is collected on a plate. Alternatively, the total beam current can be collected on a movable cone-shaped electrode inserted between the transparent and mirrored electrode. To direct the beam to the cone-shaped electrode, the mirror and transparent electrodes are held at +50 V relative to the grounded cone. (b) Detailed view of ionization region. Cold trapped lithium atoms in the MOT (red) are ionized by a UV laser (violet) and accelerated by the electric field in the source region to form the ion beam (yellow) with total current I_{total}. The amount of current that passes through the 20 µm aperture is I_{ap}.
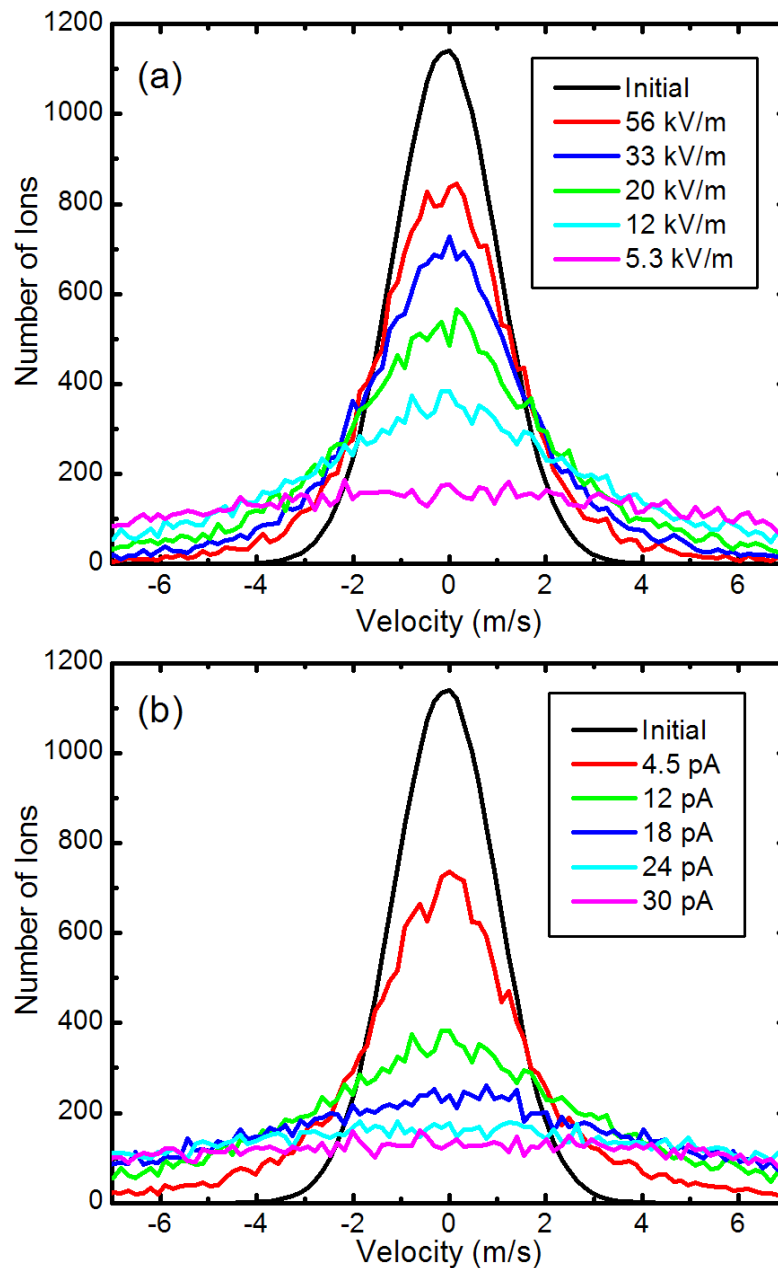
FIG 2. Transverse velocity histograms generated by Monte Carlo simulations. (a) Broadening of the transverse velocity distribution after 6 mm of flight as a function of electric field at the ion source. The lithium ions have an initial velocity distribution derived from a temperature of 1 mK. In each curve a 12 pA ion beam is being accelerated by a uniform electric field. The initial spatial distribution is Gaussian with standard deviations $\Delta x, \Delta y = 4.1\,\mu m$ and $\Delta z = 250\,\mu m$. (b) As in (a) but now holding the extraction electric field fixed at 12 kV/m and varying the beam current. 20000 ions were run through the system for each curve.
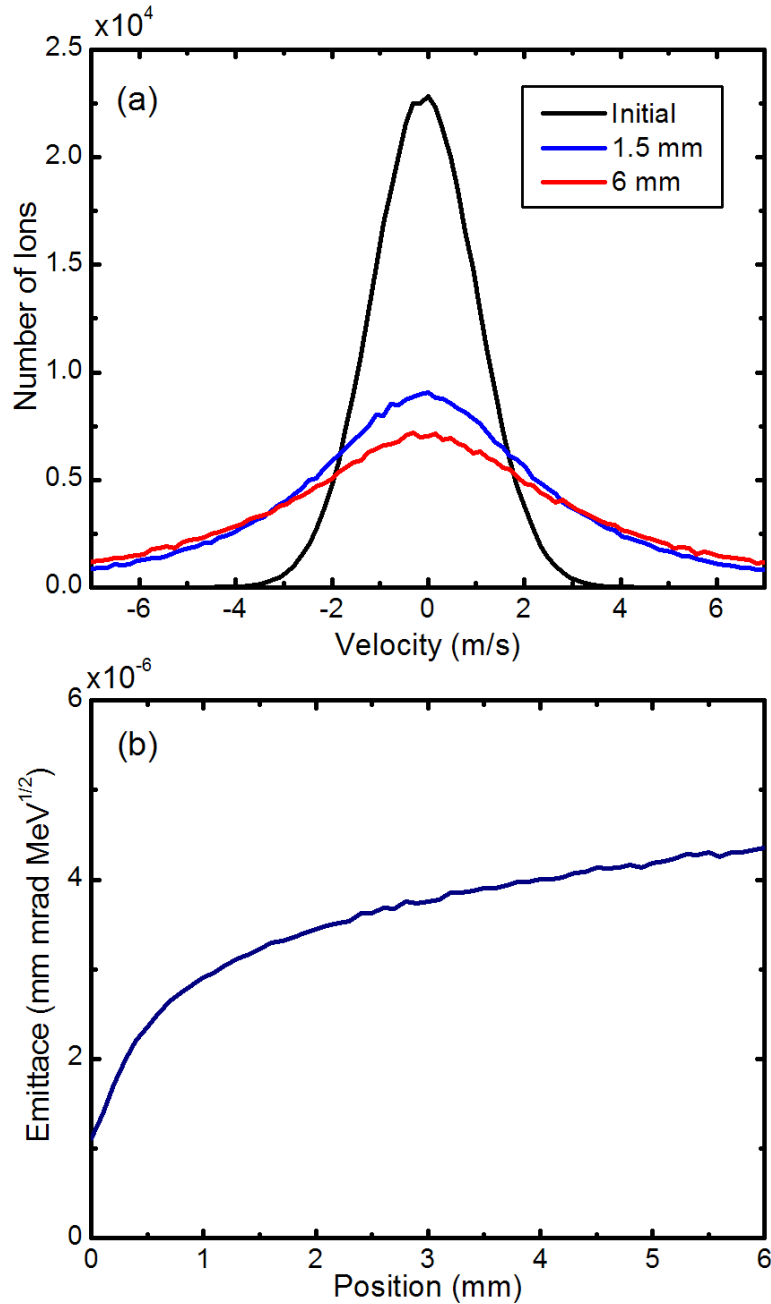
FIG 3. Monte Carlo simulated changes in transverse velocity and beam emittance as a function of distance from the center of the MOTIS along the beam propagation axis. (a) Perturbation of an initial velocity distribution as a function of distance from center of the source. Top curve represents a 1 mK lithium atom velocity distribution. Lower curves are simulations of a 12 pA beam being accelerated by a 12 kV/m electric field over the distances of 1.5 mm and 6 mm. The initial spatial distribution is as in Fig. 2. 400 000 ions were run through the system for each curve. (b) Evolution of beam emittance as a function of distance from the MOT center. Inter-ion Coulomb interactions cause the beam's emittance to increase over its propagation.
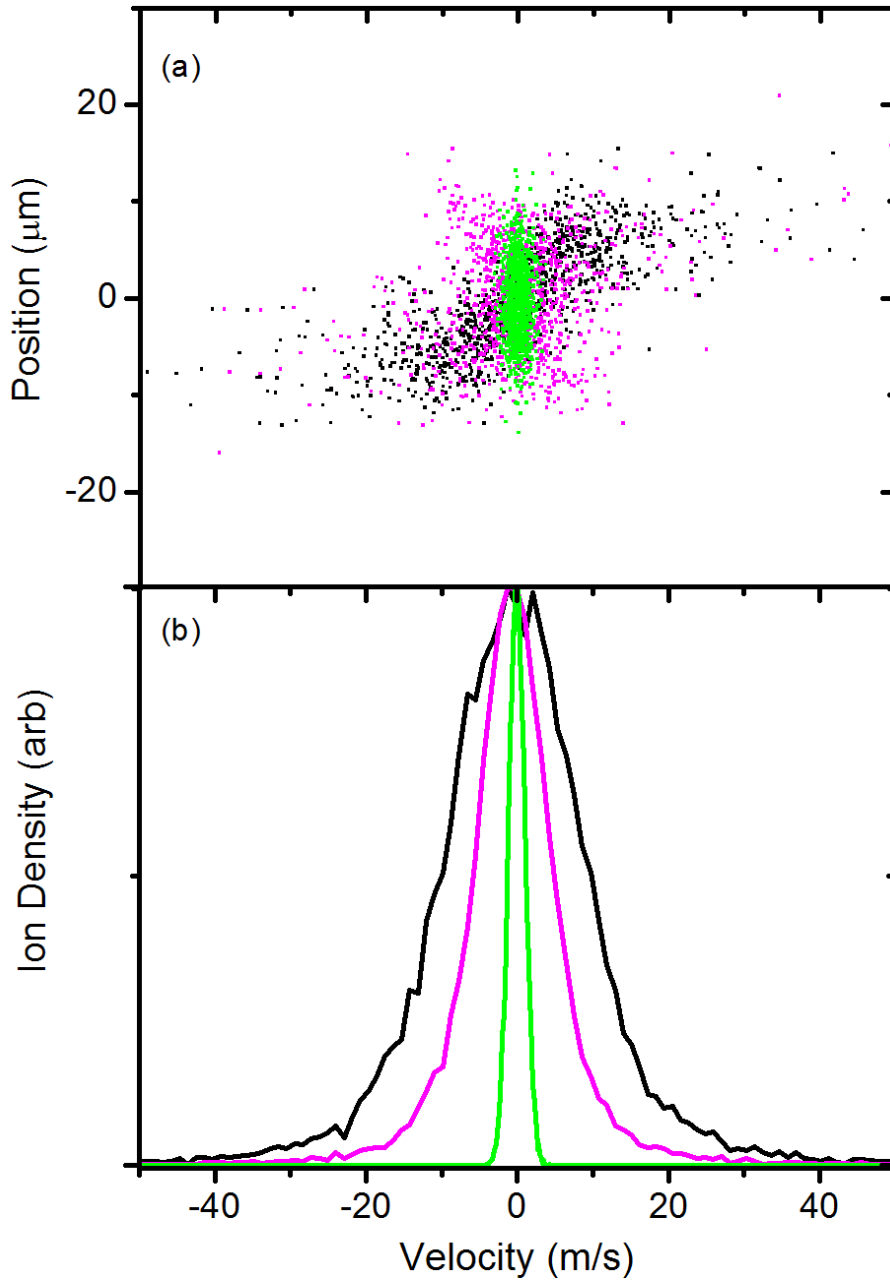
FIG 4. Phase space plots and velocity histograms for beam with 30 pA and an extraction electric field of 12 kV/m (corresponding to the 30 pA simulation in Fig. 2(b)). The initial conditions are in green. The results after the ions have traveled 6 mm are in black. The black dots after the application of a transformation to remove linear correlations between the position and velocity coordinate are in magenta. (a) Transverse coordinate velocity and position phase space graph for 1000 selected ions from a simulation of 20000 ions. (b) Velocity histograms for the same ions shown in (a). Their maxima have been normalized to more easily show the differences in curve width.
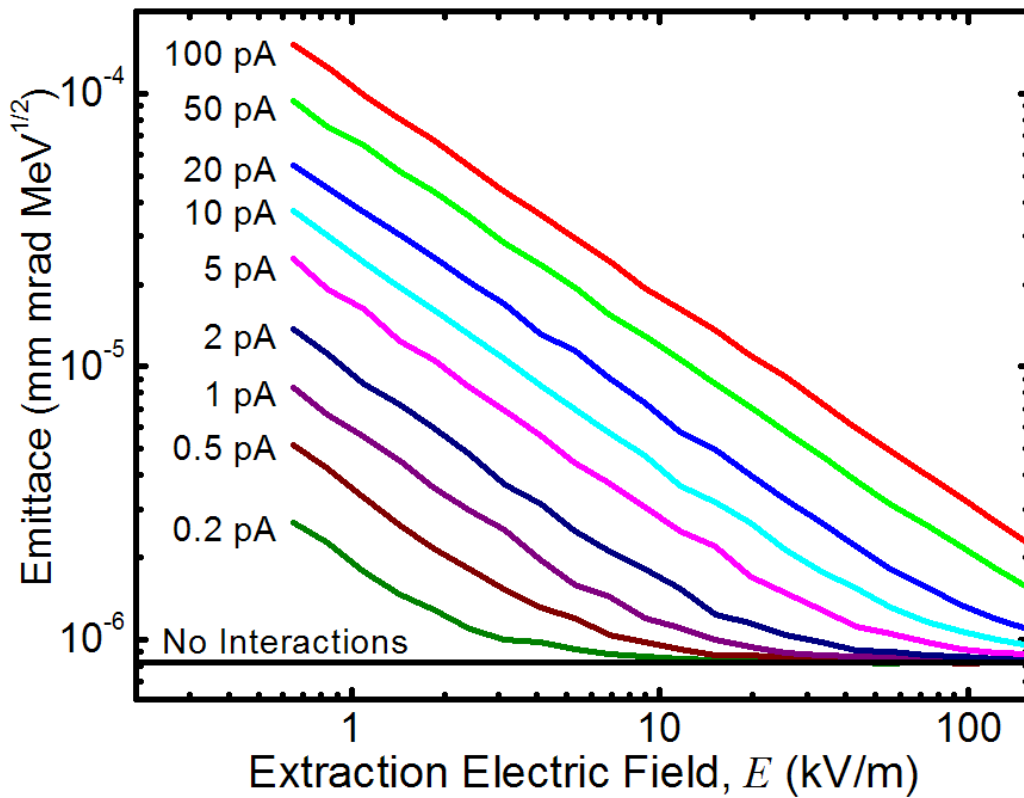
FIG 5. Monte Carlo simulated beam emittance for selected currents as a function of extraction electric field E. MOTIS geometry and temperature of the source are the same as in Figs. 1-3. At higher currents and at lower extraction electric fields the final emittance after being accelerated over 6 mm is larger than the interaction-free value. However, for a sufficiently high extraction field, all beam currents converge to the interaction-free emittance value.
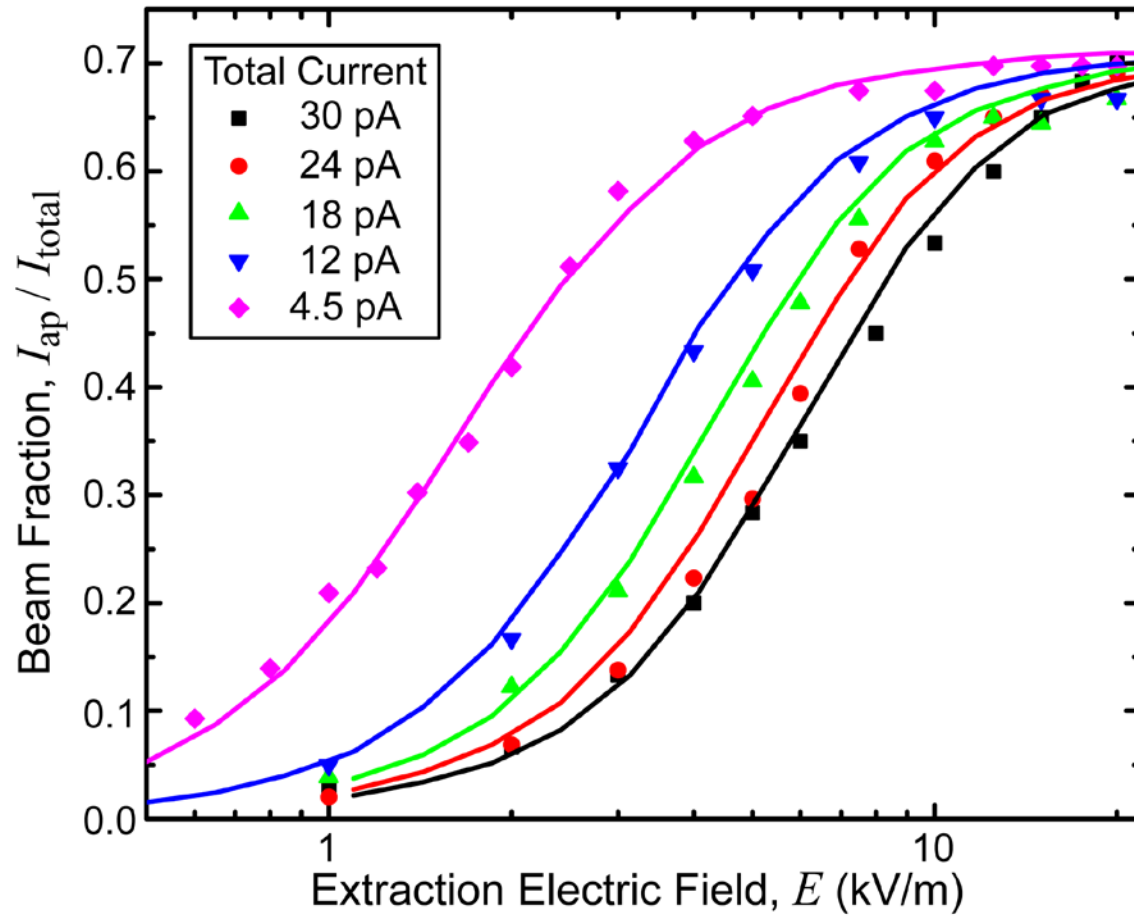
FIG 6. Fraction of beam current passing a 20 μm aperture vs extraction electric field for various beam currents. Symbols are experimental data and solid lines are Monte Carlo simulations. Uncertainties of the measured data are $\pm$ 7 %.